Thesis for The Degree of Licentiate of Technology

Optically Driven Nanomotors for Cellular Motion Detection at the Nano-Scale

A turbulent journey

Emelie Tornéus

CHALMERS
UNIVERSITY OF TECHNOLOGY

Department of Physics
Chalmers University of Technology
Gothenburg, Sweden, 2024

Optically Driven Nanomotors for Cellular Motion Detection at the Nano-Scale
A turbulent journey

Emelie Tornéus

Cover: A digital collage of images taken with dark-field microscopy of endothelial cells.

Department of Physics
Division of Nano and Biophysics
Chalmers University of Technology
SE-412 96 Göteborg,
Sweden
Phone: +46(0)31 772 1000

Printed by Chalmers Digitaltryck,
Gothenburg, Sweden 2024.

Optically Driven Nanomotors for Cellular Motion Detection at the Nano-Scale

A turbulent journey

Emelie Tornéus

Department of Physics
Chalmers University of Technology

Abstract

Studying cells, the fundamental units of life, is crucial for advancements in fields like medicine and biotechnology. Advances in cellular research are closely linked to the development of methods that can measure nanoscale biological processes, both in time and space. A particularly important area is the study of mechanical motions in single cells, which are connected to cell viability and health. To study these nanomotions, a highly sensitive, non-invasive method is essential.

This thesis presents a method for detecting nanomotions in living cells using a single rotating nanomotor trapped with optical tweezers. Optical tweezers are a popular tool used in biological research due to their ability to sense and apply minute forces and torques to microscopic objects, as well as their ease of implementation allowing for precise studies of biological samples. In this approach, a nanorod supporting plasmonic resonances is trapped in two dimensions against a glass surface and rotated through torque transfer from a circularly polarized laser beam. The rotation frequency of the nanomotor is proportional to the optical torque, which is determined by the light intensity. By manipulating the nanomotor along the beam's focus, this thesis demonstrates a near-linear relationship between its rotation frequency and position. Fluctuations of the cell membrane can displace the nanomotor along the laser beam, allowing for the detection of cellular nanomotions ranging from tens of nanometers to up to a micrometer. This opens new opportunities to study specific cellular processes, and in turn facilitating a deeper understanding of single-cell pathology.

Keywords

Optical tweezers, plasmonic nanoparticles, nanomotors, optical torque, cellular nanomotions

List of Publications

This thesis is based on the following publication:

Paper I

Detecting nanomotion patterns of single endothelial cells using light-driven rotary nanomotors
E. Tornéus, C. Hamngren Blomqvist, C. Beck Adiels and H. Jungová
Submitted

Declaration of author contributions:

Paper I

I performed all experiments, including method development, optimization, measurement of cellular nanomotions, development of data analysis procedures, and co-wrote the manuscript.

Acknowledgment

This thesis marks a milestone in a journey that I by no means made alone. I've had the support and encouragement of many people along the way, and I'm grateful to everyone who has been a part of it.

First, I would like to thank my supervisor, Hana Jungová, for inviting me on this journey in the first place. I truly appreciate all the time and guidance you've given me, as well as your enthusiasm and patience, thank you! I deeply appreciate your support during my recovery, and I especially want to thank you for being there every step of the way.

I would like to extend my gratitude to Mikael Käll, my supervisor. Thank you for all your advice along the way and for sharing your knowledge, you're truly a great teacher. I especially want to thank you for your support during my recovery.

Caroline Beck Adiels, I am very grateful for our interesting discussions and your advice on this project. To Charlotte Hamngren Blomqvist, thank you for all the time you spent on those little cells that are so important for this work, and especially for the admirable work you do in the 3rd-floor lab.

My acknowledgement extends to my examiner Fredrik Höök, for being such a big scientific inspiration and for teaching the most important course for my PhD.

My gratitude extends to those who reside, now and in the past, on the 6th floor. I especially want to thank the brilliant Pantea, Adriana, Betül, Laura and Michaela for all the support and kindness. I want to thank Timur, Sasha, Mahdi, Gosha, Julia, Mindaugas, Einstom, Erik, Abhay, Khosro, Vasilii, and Oleg for creating an encouraging atmosphere that motivates scientific endeavors, as well

as for the great conversations during our lunches and fikas.

I would like to thank all my former and present colleagues at the Nano and Biophysics department. A special thanks to Julia, who proofread this thesis and never lets me forget that I am older than her.

Kajsa, you are such an important person to me. Thank you for putting up with my occasional strokes of insanity and for being the one who can make me laugh like no other. To my dear friends Frida, Sofia, Govin, Ale, Amir, Harald, Stina, Viktor, and Emma, thank you for everything. A special thanks to my oldest friend, Sanna, and her husband, and my dear friend, Josef.

I would like to thank my parents for always encouraging and believing in me. I would also like to thank my siblings, Eleonor, Erik, and Emil, as well as my brother-in-law Matthias, the girls, and my extended family, the Kettunens. Thank you!

Johan, I am deeply grateful for you and without you there would be no thesis, thank you for putting up with me.

Emelie Tornéus
2024/09/08
Göteborg

Contents

List of Figures

Chapter 1

Introduction

In 1665, the English scientist Robert Hooke published Micrographia, a seminal book that detailed his observations of various plants and insects using a microscope [1]. In this work, Hooke introduced the term 'cell' to describe the smallest living units. While examining a piece of cork, he noted that the tiny, pore structures reminded him of the small rooms, or cells, in a monastery. This comparison led to the adoption of the term 'cells' to describe these fundamental units of life. The interest in studying cells has continued to grow over the centuries, driven by the hope of understanding life and finding ways to cure diseases. This ongoing research has led to significant advancements in biology and medicine, providing insights into cellular processes and the development of treatments for various health conditions.

Studying cells is a complex task that requires specialization in various research fields due to the intricate nature of cellular structures. Just as medical doctors have specialties that focus on different diseases, conditions or patient groups, scientists have created distinct fields such as genomics [2], transcriptomics [3], cell metabolism [4], cell signaling [5], cell death [6] and many more, to focus on different cellular functions. The methodology of cell study is also critical, whether analyzing cells as colonies or single cells, *in vivo* or *in vitro* , or studying specific cellular compartments such as DNA or lipid membranes. The advancements in cell biology is connected to the advancements in microscopy and technology, the methods used to study cells. Commonly used methods in cell biology today are for example fluorescent microscopy [7, 8], confocal microscopy [9]

or cytometry [10]. Even more specialized methods has been applied in cell biology, one of them being optical tweezers [11, 12].

Optical tweezers emerged as a suitable tool to address these challenges, as they can exert and detect forces or torques on individual micro- and nano-sized objects with piconewton precision and measure spatial displacements on the nanometer scale [13, 14, 11]. They trap and hold objects in 3D using a single focused laser beam, a technique first reported by Arthur Ashkin and co-authors in 1986 [15]. This followed Ashkin's earlier work from 1970 on transporting and trapping micron-sized beads in water through momentum transfer from a laser beam [16]. In 1987, Ashkin and co-authors demonstrated the use of optical tweezers to manipulate and study single cells, as well as organelles inside cells[17]. Ever since, numerous studies have been published using optical tweezers to explore various cellular processes and mechanics. One contributing factor to the widespread use of optical tweezers is the ability to study cells and cell compartments in real-time in a non-invasive manner. Optical tweezers have been utilized to study the mechanical properties of DNA [18], measure the forces exerted by motor proteins like kinesin and dynein [19, 20], investigate the viscoelastic properties of the cytoplasm [21, 22], and manipulate single cells to understand their interaction dynamics and adhesion properties [17, 23].

Building on the established applications of optical tweezers, my research focuses on utilizing this versatile tool in conjunction with plasmonic gold nanorods to measure mechanical, nano-sized fluctuations in single cells. The unique properties of plasmonic nanoparticles enable an enhancement of the optical forces generated by the optical tweezers, allowing for trapping with very low laser power [24]. Additionally, the resonance properties of plasmonic nanoparticles have been extensively studied for optimal trapping conditions [25, 26], as well as for understanding photothermal effects and the thermodynamics of trapped metal nanoparticles [27, 28]. Furthermore, these nanoparticles have shown potential applications as biosensors [29, 30].

A pivotal part of this thesis involves studying the rotation of gold nanorods. It is well-known that photons can exert momentum onto an object, causing it to move. However, if the laser has circular polarization, it is possible to set a trapped particle into rotation through the angular momentum exerted by the laser [31, 32]. The

optical torque exerted by spin angular momentum transfer can originate either absorption or scattering of photons, for the gold nanorods used in this work, the optical torque mainly comes from the scattering of photons, which is significantly enhanced around the particle's localized surface plasmon resonance (LSPR) [33, 34]. When the scattering becomes as pronounced as it is around the particle's LSPR, it is no longer feasible to trap the particle in 3D. Instead, a 2D trap can be created. In this setup, the particle is pressed against a surface due to light pressure but is counterbalanced by the Coulomb force acting in the opposite direction, allowing the particle to rotate freely very close to the surface [35]. For this work, the relationship between the rotation of a nanorod and its position within the laser beam is explored and utilized to measure local nano-sized fluctuations in living cells.

This licentiate thesis encompasses a theoretical background concerning light-matter interaction with an emphasis on localized surface plasmon resonance of metal nanoparticles, the principles and application of optical tweezers for metal particles, and an introduction of the mammalian cell, and more specifically the endothelial cell, including their mechanical motions and methods of study. The thesis further details the experimental procedures used in the research and concludes with a summary of the findings and a discussion of future perspectives.

Chapter 2

Plasmonics

The project presented in this thesis relies on a phenomenon called plasmons, and more specifically, Localized Surface Plasmons (LSPs), to trap gold nanorods at very low laser powers — an approach that is desirable when working with sensitive samples such as living cells.

Plasmons are collective oscillations of free electrons in a conducting media and are typically divided into three categories: bulk plasmons, where the conduction electrons oscillate through the volume of the material; Surface Plasmon Resonance (SPR), may arise at the interface between a metal and a dielectric material when an optical field is applied; and LSPs, which occur in nano-sized structures where free electrons oscillate collectively in response to light. The latter is the type of plasmons we will examine more closely in this chapter, beginning with the optical properties of noble metals, including the Drude model. We will then explore the quasi-static approximation, in which one can analytically derive optical properties for nanoparticles, and conclude with light-induced heating of gold nanoparticles.

2.1 Optical Properties of Noble Metals

The optical properties of metals can be described by permittivity, $\varepsilon(\omega)$, a complex-valued function that depends on the frequency of light [36]. For a metal, the real part of the function is usually negative and related to reflectivity of the material, while the ima-

ginary part is related to absorption of the light. The permittivity is, as a matter of fact, the only parameter we need to describe the interaction between light and a material. This is true as long as we restrict ourselves to the electric interaction of light and material, if the magnetic properties are taken into account the permeability need to be considered too. The permittivity describes the displacement of the electrons when an external electrical field $\mathbf{E}$ is applied, such as

$$\mathbf{D} = \varepsilon_0 \mathbf{E} + \mathbf{P} \tag{2.1}$$

where $\mathbf{D}$ is the displacement field, $\mathbf{P}$ is the macroscopic polarization density and ε_0 is the permittivity of free space. For a noble metal, which is non-magnetic, linear, isotropic and homogeneous, the displacement field can be expressed proportional to the electric susceptibility χ, as

$$\mathbf{P} = \varepsilon_0 \chi \mathbf{E} \qquad \Rightarrow \qquad \mathbf{D} = \varepsilon \mathbf{E}. \tag{2.2}$$

The permittivity $\varepsilon = \varepsilon_r \varepsilon_0 = \varepsilon_0(\chi + 1)$ is introduced to reach the conclusion of Equation (2.2), where ε_r is the relative permittivity, describing how a material responds to an applied electric field. The interaction between light and matter is stronger for a material with large ε_r, and vice versa if ε_r is small.

For a single frequency or wavelength, the permittivity is a constant, describing the optical properties of materials. However, the optical response of a material is dispersive and depends on the frequency of light (ω). Hence, for broad-band illumination it make sense to introduce the permittivity as a function of frequency, $\varepsilon_r(\omega)$. The function $\varepsilon_r(\omega)$ is complex-valued, as the material cannot respond to a change in the applied field instantaneously which results in a phase difference between $\mathbf{D}$ and $\mathbf{E}$.

The permittivity can be described classically with the Drude-Lorentz model [37]. Here, the electrons in the material are modeled as a damped harmonic oscillator around the fixed, positively charged ions. The displacement x of the electrons is described by the equation of motion in time as,

$$\ddot{x}(t) + \zeta\dot{x}(t) + \omega_0^2 x(t) = -\frac{e}{m_e}\mathbf{E}(x,t) \tag{2.3}$$

where m_e is the electron mass, ζ is the damping frequency, ω_0 is the resonant frequency of the system, and e is the charge of an electron. By performing a Fourier transform with respect to the angular frequency ω, we get the following expression for the dipolar polarization density

$$\mathbf{P}(\omega) = \frac{Ne^2/m_e}{\omega_0^2 - \omega^2 - i\zeta\omega}\mathbf{E}(\omega), \tag{2.4}$$

with N being the electron density. Assuming a homogeneous and isotropic material, we can write the permittivity as

$$\varepsilon_r(\omega) = 1 + \frac{\omega_P^2}{\omega_0^2 - \omega^2 - i\zeta\omega} \tag{2.5}$$

where $\omega_P = (Ne^2/m_e)^{1/2}$ is the plasma frequency.

The first term of Equation (2.5) refers to the free space response and the second term is the material's response. For a conducting metal, the restoring force (or resonant frequency $\omega_0 = 0$, in Equation (2.4)) is lost as the conduction electrons are not bound to the nuclei [38]. The permittivity becomes

$$\varepsilon_r(\omega) = \varepsilon_\infty + \frac{\omega_P^2}{\omega^2 - i\zeta\omega}. \tag{2.6}$$

The first term in Equation (2.6), ε_∞, accounts for the net contribution from the positive ion nuclei. The damping frequency $\zeta = 1/\tau$ relates to the relaxation time τ of the electrons. This is the Drude approximation of permittivity, which does not account for interband transitions between the conduction and valence bands in the atom. For gold, which is the material used in this thesis work, the interband transitions are responsible for the enhanced absorption of wavelengths below 600 nm [39]. In Figure 2.1 the real and imaginary parts of the permittivity for gold are shown together with experimentally measured data. However, for the spectral range we are interested in the Drude approximation is sufficient.

The permittivity is closely related to the more commonly used refractive index n and for a non-magnetic material it is defined as

$$n = \sqrt{\varepsilon_r}. \tag{2.7}$$

The refractive index is related to how fast light can propagate through a material and is many times referred to as optical "density". The refractive index is also complex-valued, where the imaginary part represents the attenuation coefficient describing the losses of the propagating wave in the material [38].

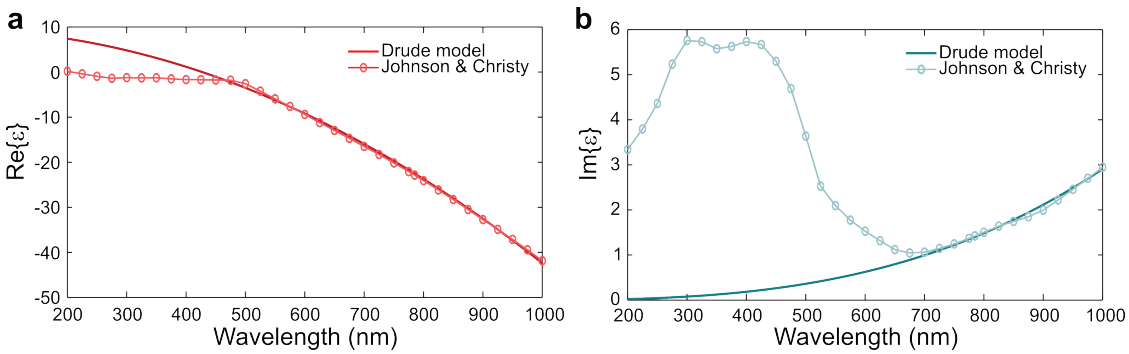

Figure 2.1: Real (**a**) and imaginary (**b**) part of the permittivity (ε) for gold, calculated with the Drude model using a plasma frequency of $1.4{\cdot}10^{16}$ (rad/s), damping frequency $1.05{\cdot}^{14}$ (rad/s) and high-frequency permittivity of 9.5 [40]. The Drude model is compared with experimentally measured permittivity by Johnson and Christy [41].

2.2 Localized Surface Plasmon Resonance

The optical properties described in the previous section are general with no imposed spatial conditions for the material. From here on, we are going to focus on light interaction of sub-wavelength particles. The plasmons we are interested in are the localized surface plasmons, which are non-propagating excitations of the conduction electrons in a material and occurs when all dimension of the material is at the nano-scale [42].

The LSPR arise when the oscillation frequency of the free electrons match the frequency of the applied electromagnetic field. For gold and silver, these resonances are within visible and infrared region of the electromagnetic spectrum, which is why these materials

have been so popular in various applications, and especially for bio-sensors [43, 44].

The LSPR is highly dependent on the size and shape of the nanoparticle, as well as the surrounding medium. When the resonance condition is met the scattering and absorption cross-sections of the particle are greatly enhanced. For a small spherical nanoparticle, a single dipole resonance is excited, but with increasing size of the nanoparticle, higher order modes arise. For small nanorods, two separate dipole modes arise, which correspond to the excitation of the transverse and longitudinal direction of the rod [34, 33]. Figure 2.2 illustrates the LSPR modes of a spherical nanoparticle and a nanorod.

For small nanoparticles with diameter (d) much smaller than the wavelength (λ) (with d up to $\sim$ 100 nm) it is possible to analytically calculate the absorption and scattering properties using a simplified model called the quasi-static approximation [42]. For an arbitrarily shaped particle or larger particles one has to turn to numerical simulations to extract the same properties [45].

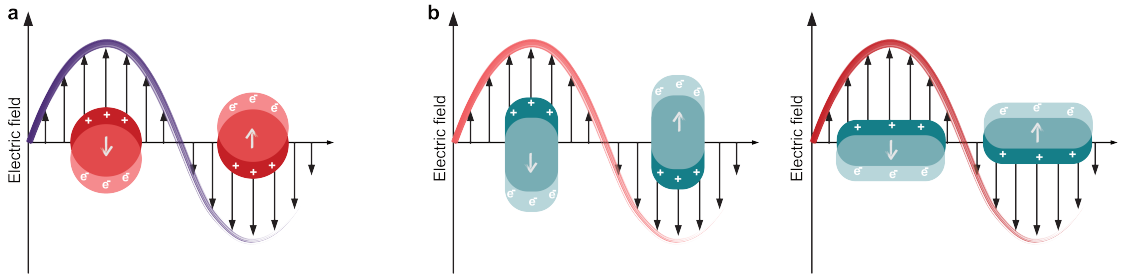

Figure 2.2: Schematic illustration of LSPR (**a**) for a spherical nanoparticle and in (**b**) for spheroidal (rod-shaped) nanoparticle with its longitudinal and transverse LSPR modes.

2.2.1 Quazi-Static Approximation

If a particle is much smaller than the wavelength of the applied electromagnetic field, one can assume that the harmonically oscillating field is constant over the particle volume. For particles larger than 30 nm, one has to expand the model to include retardation effects due to depolarization of the emission from different points on the particle. The model is called the modified long-wavelength approximation [46, 47]. Following is a brief summary of the quazi-static approximation for two types of particle shapes, a sphere and

a spheroid. The spheroidal case can be use to extract the optical properties for a nanorod analytically, which is the type of particles used in this thesis work.

Spherical Particle

A homogeneous and isotropic spherical particle with radius a is located in the origin of a uniform electrical field $\mathbf{E}$ [42]. The surrounding medium is non-absorbing and homogeneous with a permittivity ε_m and the permittivity of the particle is $\varepsilon(\omega)$. By solving the Laplace equation for the potential for the electrostatic case, one arrives at the dipole moment

$$\mathbf{p} = \varepsilon_0 \varepsilon_m \alpha \mathbf{E} \tag{2.8}$$

where α represent the polarizability of the particle

$$\alpha = 4\pi a^3 \frac{\varepsilon(\omega) - \varepsilon_m}{\varepsilon(\omega) + 2\varepsilon_m}. \tag{2.9}$$

In Equation (2.9) we can see that a resonance condition is imposed with $\varepsilon(\omega) = -2\varepsilon_m$, for a distinct frequency ω.

Spheroidal Particle

The quazi-static approximation is also applicable for spheroidally shaped particles and is a good first approximation of a nanorod. Again, the size have to be considerably smaller than the wavelength but, for this case we need to consider the semi-axes a, b and c of the particle [48]. For a prolate (cigar-shaped) spheroid, two of the axes are equal ($b = c$) and $a > b$. The dipole moment for a spheroid (j $= a, b, c$) becomes

$$\mathbf{p}_j = 4\pi\varepsilon_m abc \frac{\varepsilon_r(\omega) - \varepsilon_m}{3(\varepsilon_m + L_j(\varepsilon_r(\omega) - \varepsilon_m))} \mathbf{E} \tag{2.10}$$

where L_j represent the geometrical factor of the directions of the spheroid. For semi-axes a, L is

$$L_a = \frac{abc}{2} \int_0^\infty \frac{1}{(a^2 + q) f(q)} dq \tag{2.11}$$

and the polarizability becomes

$$\alpha_j = 4\pi\varepsilon_m abc \quad \frac{\varepsilon_r(\omega) - \varepsilon_m}{3(\varepsilon_m + L_j(\varepsilon_r(\omega) - \varepsilon_m))}. \tag{2.12}$$

The spheroid holds two separate plasmonic resonances, one for the semi minor and one for the semi major axes. The semi major axes of a spheroid can have plasmonic resonance shifted towards the infrared regime, which is especially interesting for biological applications.

2.2.2 Optical Cross-Sections

Given the quasi-static approximation, we are also able to determine the scattering and absorption of light for a nanoparticle. Again, this approximation simplifies the analysis, allowing us to derive the absorption and scattering cross-sections analytically. The scattering cross-section, σ_{scat}, determines the efficiency of the particles ability to scatter light and the absorption cross-section, σ_{abs}, determines how much of the applied light is absorbed by the particle. The extinction cross-section quantifies the total loss of intensity of the incident light due to both absorption and scattering by the particle as $\sigma_{ext} = \sigma_{scat} + \sigma_{abs}$. σ_{ext} and σ_{scat} can be expressed in terms of polarizability as

$$\sigma_{ext} = kIm\{\alpha(\omega)\} \tag{2.13}$$

and

$$\sigma_{scat} = \frac{k^4}{6\pi}|\alpha(\omega)|^2. \tag{2.14}$$

Here, $k = 2\pi n_m/\lambda_0$, n_m is the refractive index of the medium and λ_0 is the wavelength in free space [42].

2.2.3 Light-Induced Heating of Gold Nanoparticles

The light absorbed by plasmonic nanoparticles primarily dissipates as heat to their environment. At a wavelength close to the plasmon resonance, both the scattering and absorption of light are significantly enhanced, leading to increased heat generation. In fields like thermoplasmonics the heat generation of nanoparticles is the means

for a system [49, 50, 51], while in biology it can be used as a tool to reach a specific goal, such as thermal cancer treatment [52, 53], or it is an unwanted side effect in heat sensitive systems. Nonetheless, heat is often an inevitable effect of light-matter interaction.

A spherical nanoparticle under light irradiance I, transforms light energy into heat Q as $Q = \sigma_{abs} I$ [54]. When the particle is metallic and much smaller than the incoming wavelength, one can assume that the particle has a uniform temperature, T_{np}, that under steady-state conditions for a spherical nanoparticle is described by

$$T_{np} = T_{env} + \frac{\sigma_{abs} I}{4\pi a \kappa}. \tag{2.15}$$

Here, T_{env} is the temperature of the environment, a is the particle radius and κ is the thermal conductivity of the surrounding medium. Equation (2.15) shows that the temperature of the nanoparticle is directly proportional to the absorption cross-section and the light intensity. The dissipation of the heat from the nanoparticle to its environment depends on thermal conductivity of the surrounding medium [54]. Again, this is the most simple model for temperature of a metallic nanoparticle and for other shapes and sizes numerical simulations are required.

Chapter 3

Optical Tweezers

In this chapter, we will explore optical tweezers, the primary tool used in the method discussed in this thesis. We will begin with an introduction to the optical forces that govern the system, focusing on metallic nanoparticles and how these forces are calculated using the dipole approximation. Following that, we will examine the random motions a particle experiences when optically trapped, specifically translational and rotational Brownian motion. We will then briefly touch on surface interactions, concluding with a discussion on how photons transfer angular momentum to an optically trapped nanoparticle.

3.1 Optical Forces

When a single laser beam is focused into a small spot, the optical forces in such a setup create a potential well that can attract and capture micro- and nano-sized objects in 3D. This is what we call optical tweezers, a tool that has become widely used in biology, physics, and materials science for experiments requiring the manipulation of very small objects.

In optical tweezers, photons interact with a trapped particle via elastic and inelastic collisions, exerting a force, F, on the particle. The force experienced by the particle is the sum of two forces: the gradient force, $\mathbf{F}_{grad}$, and the scattering force, $\mathbf{F}_{scat}$. The gradient force is a conservative force that will guide the particle within the gradient of the electromagnetic field, and is responsible for confining

the particle in the trap. The scattering force, a non-conservative force, acts along the propagation direction of the incoming light and is a result of the scattering and absorption processes, proportional to the intensity of the of light. To be able to confine a particle in 3D, the gradient force must overcome the scattering force and the potential well of the trap must be equal to or larger than the particle's thermal energy resulting from Brownian motion [55].

Trapping metallic particles, a process central to the research presented in this thesis, has distinctive optical properties compared to trapping dielectric particles. Metallic particles possess free conduction electrons, which can oscillate under an optically applied field, generating plasmons, as described in Chapter 2. For metallic particles at the nanoscale, these oscillations are subjected to a restoring force due to the positive charge of the nuclei, resulting in resonances in the optical response known as LSPs. These LSPs demand special consideration when designing optical tweezers. If 3D trapping is desired, one may detune the laser from the LSPR wavelength of the particle to reduce the enhancement of absorption and scattering due to LSPR [24]. In this work, however, the opposite is desired, the LSPR of the trapped particles is tuned to match the laser wavelength, resulting in an enhanced scattering force. The trapped particle cannot be confined in 3D by the gradient force alone, but is pushed along the optical axis towards the cover glass, where it is counterbalanced by Coulomb repulsion from a surface with the same charge polarity as the particle itself [33, 34, 35].

3.1.1 Dipole Approximation

To calculate the force generated by optical tweezers on a particle with an arbitrary shape, the Maxwell stress tensor is integrated over a confined surface containing the particle, using computational approaches such as Mie theory or finite difference time domain (FDTD) simulations [36]. However, for metallic particles much smaller than the trapping wavelength, the dipole approximation can be applied to describe the optical forces in the system [55].

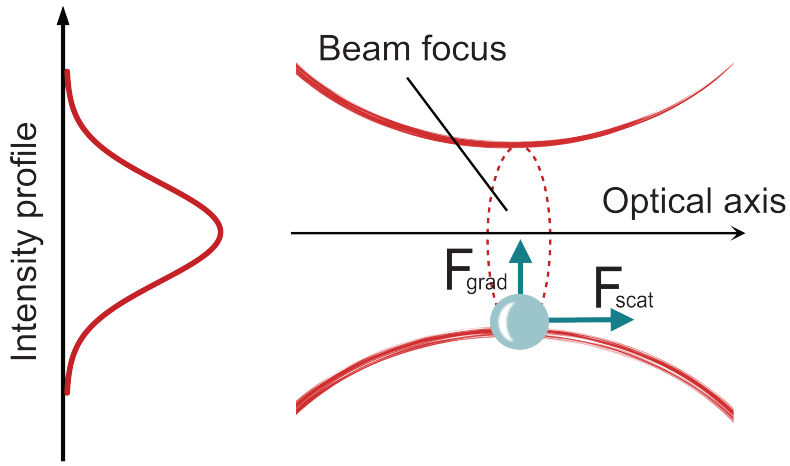

Figure 3.1: An optically trapped particle smaller than the wavelength of light experiences a scattering force, $\mathbf{F}_{scat}$, that pushes the particle along the direction (optical axis) of the light's propagation, and a gradient force, $\mathbf{F}_{grad}$, that guides it towards the focus, i.e., the area of highest light intensity in the case of a Gaussian beam profile.

In the dipole approximation, as the name suggests, the particle is regarded as an oscillating dipole induced by the oscillating electromagnetic field from the optical tweezers. The optical force experienced by the dipole is a Lorentz force, with a linear relationship between the induced polarization $\mathbf{p}$ and the electric field $\mathbf{E}$. This means that the total optical force can be decomposed into gradient and scattering force components, $\mathbf{F} = \mathbf{F}_{grad} + \mathbf{F}_{scat}$, expressed as follows:

$$\mathbf{F}_{grad}(r) = \frac{1}{2\epsilon_0} Re\{\alpha\} \nabla I(r) \tag{3.1}$$

$$\mathbf{F}_{scat}(r) = \frac{n_m}{c} \sigma_{ext} \langle S(r) \rangle \tag{3.2}$$

where r denotes the position of the particle and $\langle S(r) \rangle$ is the time-averaged Poynting vector [34]. In Equation (3.2), we observe that the force is proportional to σ_{ext}, indicating that $\mathbf{F}_{scat}$ is non-conservative, as it describes the momentum transfer from the field to the particle due to scattering and absorption processes (Figure 3.1) [55].

Here, we can see that the conservative gradient force can either attract or repel particles from the optical trap. If a particle has

positive polarizability, meaning it has a higher refractive index than the surrounding medium, it will be attracted to the high-intensity regions of the trap. Conversely, a particle with a lower refractive index than the medium will be repelled [55]. The polarizability of plasmonic particles is also influenced by the relationship between their LSPR and the laser wavelength. If the LSPR is on the lower flank of the laser wavelength, the polarizability becomes positive and, if it is higher than the wavelength, the polarizability may become negative [56].

3.1.2 Trap Stiffness

The confinement of an optically trapped particle depends on the optical forces exerted by the laser and the thermally induced fluctuations of the particle [55]. For a particle with a higher refractive index than the surrounding medium, the laser creates an attractive potential well that pulls the particle to the center of the trap, while the particle continuously experiences random displacements due to Brownian motion. This force balance can be estimated using Hooke's law:

$$F \approx \kappa_x(x - \bar{x}_{eq}) \tag{3.3}$$

where, x is the displacement, $\bar{x}_{eq}$ is the equilibrium position and κ is the spring constant, also known as the trap stiffness. Calibrating an optical tweezers system is based on determining the trap stiffness. There are different methods to experimentally measure the trap stiffness, with the power spectrum method and the equipartition method being two common approaches [57].

3.2 Random Motion in Optical Traps

Particles suspended in a fluid exhibit fast oscillatory motion, a phenomenon first observed by Robert Brown in 1827 while studying pollen submerged in water. This motion, later named Brownian motion in his honor, results from continuous collisions with the molecules in the fluid, which move due to their thermal energy and not from any external perturbations of the particles [58]. By adding a stochastic force, $\chi(t)$, to Newton's equation, one obtains the Langevin equation for translational Brownian motion, as

$$m\ddot{r}(t) + \gamma_t \dot{r}(t) = \chi(t) \tag{3.4}$$

where m is the mass of the particle and γ_t is the particle's friction coefficient for translational motion determined by Stoke's law for low Reynolds numbers, $\gamma_t = 6\pi\eta a$ for a spherical particle with radius a and η is the viscosity of the fluid which can be described with an Arrhenius type of equation [31, 59]. The stochastic force $\chi(t)$ is uncorrelated with the particle position and has a zero mean, $\langle \chi(t)x(t) \rangle = 0$ and $\langle \chi(t) \rangle = 0$.

If a particle is subjected to an external force, such as an optical force generated by optical tweezers, the Langevin equation becomes

$$\dot{r}(t) = -\frac{1}{\gamma_t} F(r) + \sqrt{2D_t} W(t). \tag{3.5}$$

Here, the term $W(t)$ represents white noise with an intensity of $2D_t$, where $D_t = k_B T/\gamma_t$ is the diffusion coefficient [55]. Due to the low Reynolds regime the accelerating term in Equation (3.4) is dropped, as the speed of the object is solely determined by the forces acting on it in the moment [55, 60].

In addition to translational Brownian motion, a particle also experiences rotational Brownian motion. This phenomenon occurs due to collisions with surrounding molecules, causing the particle to randomly change its orientation. Rotational Brownian motion is particularly important when trapping non-spherical particles, such as rods or ellipsoids, as the rotational diffusion coefficient varies along different axes of the particle. The rotational Brownian motion can also be described by a Langevin equation, but in this case, it includes an externally applied torque M_{ext},

$$\dot{\phi}(t) = -\frac{M_{ext}(r)}{\gamma_r} + \sqrt{2D_r} W(t), \tag{3.6}$$

where, ϕ is the rotation angle of the particle and γ_r and $D_r = k_b T/\gamma_r$ are the rotational friction coefficient and diffusion coefficient of the rotational motion, respectively [33, 55, 61].

3.3 Surface Interactions

The optically trapped nanorods used in this thesis have their LSPR very close to the trapping laser's wavelength, which significantly enhances the scattering force and overpowers the gradient force in the direction of the laser beam. As a result, the particles are pushed against the glass surface of the sample chamber, where the scattering force is counterbalanced by the Coulomb force, shown in Figure 3.2. In Dr. Daniel Andrén's work, described in reference [35], the DLVO theory is used to explain surface interactions in a very similar setup.

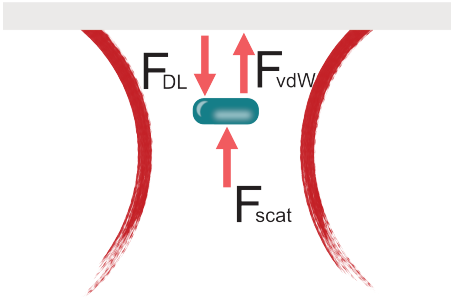

Figure 3.2: An optically trapped plasmonic nanorod with its LSPR close to the laser wavelength becomes pushed against the sample chambers cover glass by the enhanced scattering force ($\mathbf{F}_{scat}$) , where it is counterbalanced by the Coulomb force or the repulsive double layer force($\mathbf{F}_{DL}$). At very short distances the attractive van der Waals force ($\mathbf{F}_{vdW}$) also becomes a contributing factor in the system.

The DLVO theory describes how charged surfaces interact in aqueous solutions. The forces that the nanorod experiences are the Coulomb force (electrostatic force) and the van der Waals force. The van der Waals force is an attractive force that dominates at very short distances between the particle and the surface. The Coulomb force becomes repulsive if the particle and and the surface has the same charge and results from the ionization of a material's surface atoms or the absorption of ions from the surrounding environment. This leads to ions with the opposite charge accumulating around the surface, either by binding to the surface ions or by forming a diffuse electric double layer. It is the double layer that is responsible for the repulsive forces between the surfaces [62].

3.4 Optically Induced Rotation of Nanoparticles

Light can carry two different types of angular momentum: spin angular momentum (SAM) and orbital angular momentum (OAM) (illustrated in Figure 3.3). The optical torque exerted through SAM is due to the polarization state of the light and typically causes a particle to rotate around its own axis. In contrast, OAM transfers optical torque via its phase front, leading the object to move around the optical axis [63]. In the work presented in this thesis, the optical torque results from SAM transfer. The fundamental physics of SAM-induced rotation of nanoparticles is discussed in reference [31, 33, 34].

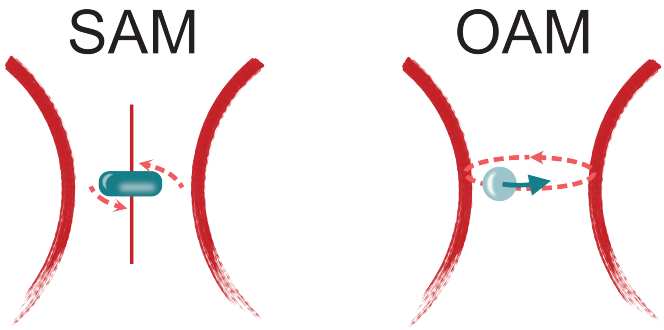

Figure 3.3: Illustration of photon induced rotation of nanoparticles. Spin Angular Momentum (SAM) of the circularly polarized laser light is transferred to a nanorod through photon absorption or scattering. Orbital Angular momentum (OAM) is transferred to a nanoparticle through the phase construction of laser beam.

3.4.1 Rotation of Nanorods

In the experimental setup used for the thesis project, a spheroid particle is trapped against the cover glass, where the Coulomb force counterbalances the plasmon-enhanced scattering force. This equilibrium allows the particle to freely rotate around one axis. This rotation is induced by the SAM through the circular polarization of the trapping laser. The equation of motion for rotation around one axis is

$$J\dot{\varphi}(t) = M_{opt} + M_f + M_s \tag{3.7}$$

where J is the moment of inertia for the particle and φ is the orientation angle. The optical driving torque is denoted M_{opt}, M_f is the counter acting friction torque from the surrounding media and

M_s is the stochastic torque generated by the rotational Brownian motion of the particle [31, 33, 34].

The optical driving torque M_{opt} is composed of scattering and absorption torques, such that $M_{opt} = M_{scat} + M_{abs}$, where $M_{abs} = \sigma_{abs} \cdot I_{inc}/\omega_0$ for a light intensity of I_{inc}, photon energy $\hbar\omega_0$ and particle absorption cross section σ_{abs}. The scattering component of the total torque can be calculated as $M_{scat} = M_{opt} - M_{abs}$. M_{opt} can be expressed as

$$M_{opt} = \langle \mathbf{p} \times \mathbf{E} \rangle \tag{3.8}$$

with $\mathbf{p}$ being the induced dipole moment and $\mathbf{E}$ the electric field. The M_{opt} can be calculated analytically if $\mathbf{p}$ can be estimated using the dipole approximation or by using Mie theory. If the particle geometry becomes more complex, a numerical approach using Maxwell's stress tensor to calculate the $\mathbf{E}$-field can be used [64].

Equation (3.8) can be used to calculate the optical torque for different types of induced E-fields. For circularly polarized incident field, with an angular frequency ω, $\mathbf{E} = (\hat{x}cos\omega t + i\hat{y}sin\omega t)E_0/\sqrt{2}$, M_{opt} for an spheroidal particle with polarizability α becomes

$$M_{opt} = \hat{z}\frac{n_m^2}{2} Im[\alpha]|\mathbf{E}|^2. \tag{3.9}$$

This corresponds to an angular momentum equal to $\hbar$ for each absorbed photon being transferred to the trapped particle, causing it to rotate around the z-axis.

The friction torque M_f for a spheroidal particle with laminar flow can be calculated through

$$M_f = -\pi\eta L^3 \varphi g, \tag{3.10}$$

where $\eta = \eta(T)$ is the temperature depended dynamical viscosity of the surrounding medium, L is the length of the particle and g is the geometrical factor of the trapped particle [65]. For a sphere $g = 1$, but for a spheroid the geometrical factor depends on its eccentricity ξ_0 and is calculated via

$$g = \frac{-e^3}{-2\xi_0 + (\xi_0^2+1)\hat{\xi_0}} \cdot \left[2\xi_0(\xi_0^2-1)tanh^{-1}\left(\frac{1}{\xi_0}\right) + \frac{-4+8\xi_0^2-3\xi_0(\xi_0^2-1)\hat{\xi_0}}{3} \right], \quad (3.11)$$

where $\xi_0 = \frac{1}{e} = \frac{1}{\sqrt{1-\left(\frac{b}{a}\right)^2}}$, with a and b being the semi-major and -minor axis of the particle and $\hat{\xi_0}$=ln$\left(\frac{\xi_0+1}{\xi_0-1}\right)$.

At steady state, when M_{opt} is counter balanced by M_f, an average rotation frequency of the particle can be expressed as [33]

$$f_{avg} = \frac{M_{opt}}{2\pi^2\eta g L^3} = \frac{M_{opt}}{2\pi\gamma_r}, \quad (3.12)$$

where $\gamma_r = \pi\eta g L^3$ and is called the rotational friction coefficient. The thermal stochastic torque M_s also affect the rotation of the particle. M_s increase in strength with increasing friction and temperature [31, 33, 34].

Chapter 4

Nanoscale Movements in Living Cells

The aim of this project is to measure the mechanical nanomotions of cells. This chapter is therefore dedicated to cells and their various processes. First, we will take a closer look at the mammalian cell and its different compartments. Since the measurements presented in the appended paper are conducted on endothelial cells, the purpose and significance of endothelial cells in the body are discussed. The last section of the chapter covers the mechanical motions generated by cells and how they have been measured and studied previously.

4.1 Cellular Structures and Endothelial Cells

The cell is the smallest living building block for all kinds of life on earth. There are two main cell categories, eukaryote cells and prokaryote cells. Both types consists of membrane enclosed cytoplasm, in which organelles with specific functions are found. The prokaryote cell is the simplest form of life, such as bacteria and archaea [66]. In contrast to eukaryotic cells, prokaryotic cells do not have a nucleus and are considered unicellular, meaning that they do not build larger multi-cellular structures, while eukaryote cells are responsible for our organs and tissues in our bodies.

Endothelial cells (ECs) are a type of eukaryote cells or mammalian cells which are specifically found in blood and lymphatic vessels [67]. They are very adaptable cells and modify their count and shape

depending on the local requirements, as they form the endothelium, which covers the inside of all vessels, from the large arteries and veins to the smallest capillary [66]. ECs are typically very flat and their thickness vary between 0.1 to 1 μm [68].

As for all mammalian cells (shown in Figure 4.1), the EC consist of a nucleus, which contains the cell's genetic material. Around the nucleus, organelles such as the endoplasmic reticulum, which synthesizes proteins and lipids, and the Golgi apparatus, which modifies, sorts, and packages proteins and lipids for secretion or delivery to other organelles, are situated. A cytoskeleton that shapes and direct the cell, as well as mitochondria that fuels the cell, to mention a few organelles and their functions [66].

ECs are responsible for the remodeling and repair of blood vessels, as well as transport liquids across semipermeable barriers and function as a barrier between tissues and the circulating blood [68]. Studying endothelial cells is crucial for understanding and treating diseases such as atherosclerosis [69], hypertension [70], and diabetics [71], where endothelial dysfunction plays a central role in disease progression and complications. Moreover, in understanding the effects of therapeutic treatments, heterogeneity of single cells plays an important role in disease progression and therapeutic failure [72]. This is why we need methods to study single cells, as it allows for more precise and detailed insights into cellular function and variability.

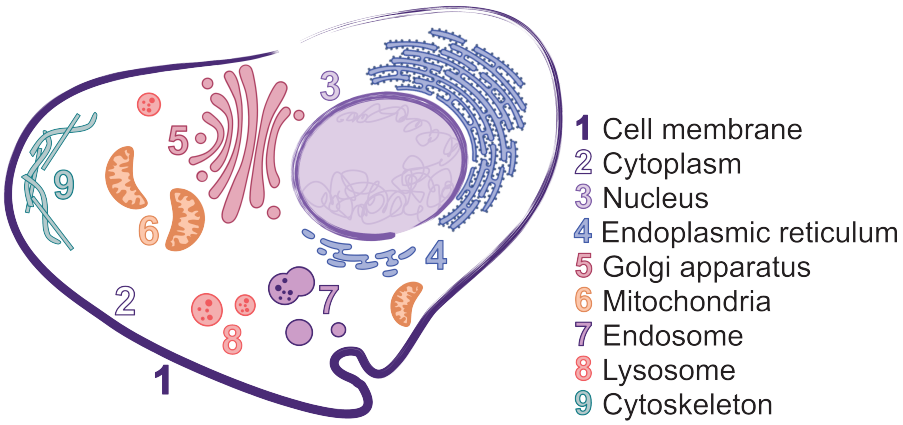

Figure 4.1: Illustration of a mammalian cell highlighting its various cellular compartments.

4.2 Mechanical Nanomotions of Cells

Cellular mechanical nanomotions refer to the small, occasionally periodic movements that occur within cells, on their surfaces, or involve the movement of the entire cell [73, 74]. These movements can be driven by various cellular processes, including metabolic activities, cytoskeletal dynamics, endoplasmic reticulum dynamics, and interactions with the extracellular environment[75, 76, 77]. By studying the cellular nanomotions we are able to gain insights into cellular functions and behaviours.

The dynamics of intracellular processes range from ideally stochastic, as seen in the diffusion of small molecules, to directed and deterministic, as found in processes like cell division. However, most intracellular biological processes lie somewhere in between or involve contributions from both deterministic and stochastic dynamics [78]. The speed or frequency of these motions depends heavily on the underlying processes and the urgency for the cell to transport a subcellular structure. If there is no rush or urgency, the cell utilizes the ever-present thermal noise for diffusion, incurring a very low energetic cost. This type of dynamic governs processes such as signaling cascades or the organization of the mitotic spindle in eukaryotic cells [79]. When a more urgent delivery is needed, active transport is carried out by the cell using energy sources like ATP or GTP. Active transport is driven by various types of molecular motors: on the cytoskeleton, there are molecular motors such as myosin or actin; on microtubules, there are kinesin and dynein. Rotary molecular motors are also found in the cell membrane, including ATP synthase and flagellar motors. Some of the fastest motions measured within a cell are of active transport of endocytic organelles, which reached speeds up to 8 μm/s [80]. The highest speeds found in cells are associated with kinesin and dynein molecular motors, which transport vesicles and organelles along microtubules. These motors have been measured to move at speeds ranging from 1-2 μm/s [81, 82, 83].

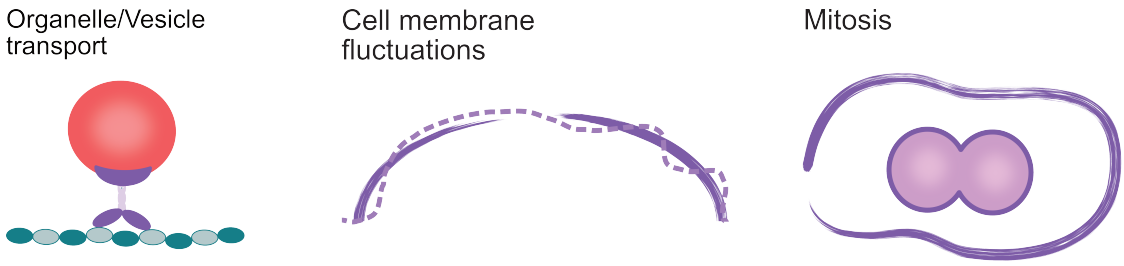

Figure 4.2: Three types of cellular process that cause mechanical motions within the cell: organelle or vesicle transport that can reach speeds up to 2 μm/s; membrane undulations or flickering that moves with speeds around 30 nm/s and mitosis which alter the cell shape significantly but at a very low speed.

Generally, the larger the organelle, the slower the motion. This is because the cell is a densely packed structure, and larger particles require more energy to move. Mitochondria, the power plants of the cell, have a distribution of mean speeds varying between 10 of nm/s to hundreds of nm/s [84]. The largest cellular organelle is the nucleus, whose motions are driven by the cytoskeleton. These motions are generally very slow, with occasional bursts that can reach up to 300 nm/s [85, 86].

Aside from organelle and vesicle transport, there are other categories of motions related to the membrane and the overall shape of the cell. The dynamics of the cell membrane are linked to the coordinated motion of all internal cellular compartments near the region [87]. Membrane undulation can be a result of thermal fluctuations, also called flickering[88], or is directed by its connection to the cytoskeleton and the speed of cytoskeletal restructuring [89], which is about 30 nm/s [78]. An additional cause of membrane dynamics is clathrin-mediated endocytosis, in which the membrane curves inward with a radius of approximately 50 nm to retrieve extracellular fluids into the cell in the form of a vesicle, a process that takes about 10 s [90]. The slower movements, those less than 50 nm/s, are usually associated with global changes in the cell shape such as cell division or cell death [78] (Figure 4.2).

Mechanical properties and nanomotions of cells are often altered in disease states. For example, changes in the mechanical properties of cancer cells can influence their ability to migrate and invade tissues [91]. Monitoring how cells respond mechanically to drugs can provide insights into the efficiency of treatments, such as predicting how cancer cells will respond to chemotherapy [92]. Additionally, assessing the antibiotic susceptibility of bacteria can be based on their motility [93, 94, 95].

4.2.1 Nanomotion Detection Techniques

A regularly applied method to study living cells is fluorescence microscopy. By using dyes such as Green Fluorescent Protein (GFP), one can study the dynamics of different cellular compartments down to the molecular level in living cells. However, the emerging field of cellular nanomotions has spurred the development of many innovative techniques for motion detection in cells. Atomic force microscopy (AFM) was one of the first methods used for this purpose. To detect nanomotions of living cells using AFM, a single cell (or an assembly of cells) adheres to the cantilever. The vibrations generated by the cell are transferred to the mechanical cantilever, creating mechanical noise in the AFM signal [93, 95]. Nanomotions of yeast cells have been studied using optical detection by tracking the x-y position of a cell with a cross-correlation image registration algorithm, a method named Optical Nanomotion Detection (ONMD) [96]. Another method developed to study the mechanical motions of cells is Tissue Dynamics Spectroscopy (TDS), where a spheroidal tumor sample is subjected to Doppler fluctuation spectroscopy, generating a spatial map of the dynamic biomarkers [97]. Live-cell imaging with super-resolution microscopy has been used to study the peripheral endoplasmic reticulum, revealing that it consists of tubules at varying densities instead of sheets [76]. Moreover, an alternative method based on graphene nanodrums was developed to measure nanomotions of single bacteria [94]. These are some techniques used for detecting cellular motions, ranging from the nano to the micrometer scale.

Chapter 5

Experimental Methods

This chapter describes the methods and procedures used to obtain the results presented in the appended paper. It covers the experimental techniques, including a description of the optical tweezers setup and dark-field microscopy. Providing an approach for exploring cellular dynamics at the nanoscale.

5.1 Optical Tweezers and Trapping in 2D

The method is based on a rather simple optical tweezers configuration. The construction is built around a Nikon Eclipse TE300 inverted microscope with a white-light dark-field illumination for dark-field imaging and detection of nanoparticles. Figure 5.1 shows a schematic illustration of the trapping setup. The laser used in this set-up is an Xtra 2, diode laser (Toptica Photonics) with a wavelength of 785 nm. The laser is collimated and directed into the microscope through a beamsplitter and, thereafter is directed via a dichroic mirror through an objective to the sample.

Before entering the microscope, the parallel polarisation of the laser is converted to circular polarization through half-wave plate ($\lambda/2$) and a quarter-wave plate ($\lambda/4$). This enable the rotation of the gold nanorod due to transfer of angular momentum from the laser to the nanorod. The gold nanorod becomes trapped in 2D against the upper cover glass of the sample chamber due to the large scattering cross-section of the nanorod. The path of the back-scattered light from the nanorod goes through the objective and

out from the microscope, where it is directed by the beamsplitter and mirrors to the fiber that collects the light for the single-photon counting photomultiplier tube (PMT) that enable us to record the auto-correlation function of the rotational dynamics of the nanorod. This type of 2D optical tweezers setup has been used for several other publications [30, 33, 35, 61]; you can find a more in-depth description of the practical details in these references.

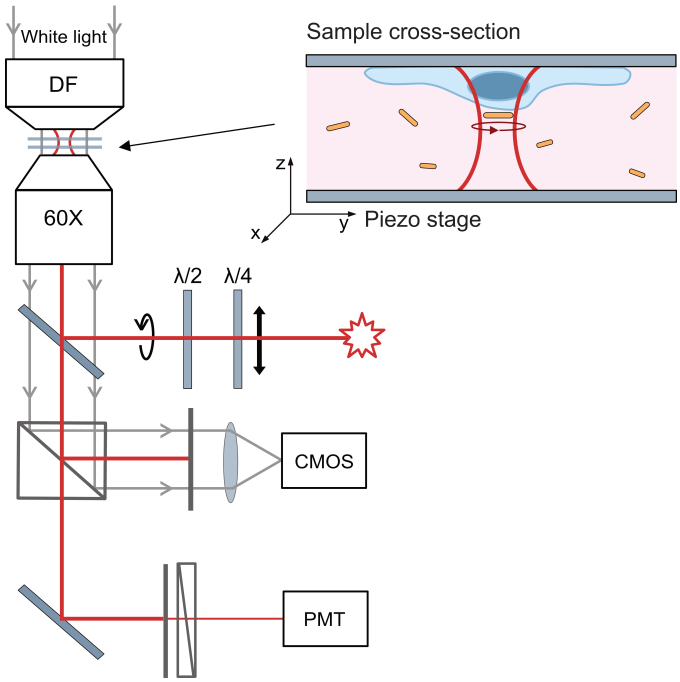

Figure 5.1: Schematic illustration of the optical setup: the inverted microscope enables trapping of a single gold nanorod against the upper cover glass of the sample chamber. Rotation of the nanorod is induced through spin angular momentum transfer, generated by a circularly polarized near-infrared laser beam ($\lambda = 785$ nm). The trapped particle is illuminated from above by a white light Dark-Field (DF) condenser. Laser light scattered from the particle passes through a dichroic beam-splitter and appropriate filters before being collected by a fiber-coupled photomultiplier tube (PMT), which is connected to a hardware correlator for particle movement analysis. The sample is mounted on a 3D piezo stage and visualized using an sCMOS camera. To the right is an illustration of the sample cross-section, showing cells adhered to the upper surface with a single nanomotors trapped on it and gold nanorods dispersed in the cell media.

5.1.1 Rotational Dynamics of a Nanorod

5.1.1.1 Auto-Correlation Function

The anisotropy of the nanorod generates two different plasmonic modes, as described in Chapter 2. The longitudinal LSPR of the nanorod is optimized to be slightly blue-shifted with respect to

the laser wavelength [56]. As the nanorod rotates around its short axis, the rotation is determined by the back-scattered light from the longitudinal axis and its corresponding polarization.

The back-scattered light is collected through a linear polarizer and the nanorod's longitudinal axis will align twice during one revolution. Hence, the intensity fluctuations of the measured signal vary twice as fast as the rotation frequency of the nanorod. By performing autocorrelation of the intensity signal we will get an exponentially decaying periodic oscillating autocorrelation-function (ACF). The ACF show the correlation between two values of the signal as their separation changes, which means that the ACF quantifies the similarity between a signal and a delayed version of itself as a function the delay or lag. This generates information about a signals repetitive patterns, if there are any, and indicate how fast a signal looses its correlation through a decay rate, which helps characterizing and interpret a signal [98]. The ACF of a rotating nanorod is described as

$$C(\tau) = I_0^2 + 0.5 I_1^2 \exp\left(-\frac{\tau}{\tau_0}\right) \cos(4\pi f \tau), \tag{5.1}$$

where I_0 represents the average intensity, I_1 denotes the amplitude of intensity fluctuation, f stands for the average rotation frequency, and τ_0 represents the autocorrelation decay time [31]. τ_0 is closely related to the rotational Brownian motion and is expressed as

$$\tau_0 = \frac{\gamma_r}{4 k_B T_r}. \tag{5.2}$$

Here, T_r denotes the rotational Brownian temperature, k_B represents Boltzmann's constant, and $\gamma_r(T)$ is the friction coefficient given by $\pi\eta(T)gL^3$. $\eta(T)$ represents the temperature-dependent dynamical viscosity of the surrounding water, g represents a geometrical shape factor dependent on the nanorod eccentricity, and L denotes the length of the nanorod.

5.1.1.2 Short-Time Fourier Transform

The PMT collects the back-scattered photons with a frequency of 100 kHz. For a measurement with a collection time of 0.5 s, we get

50 000 data points. The ACF of the signal gives very precise information about the periodicity of the signal and generates one rotation frequency and one decay time for whole collection time. However, the signal also inhibit information about the rods rotation dynamics on a shorter time scale and to extract that information we analyse the signal using Short-Time Fourier Transform (STFT).

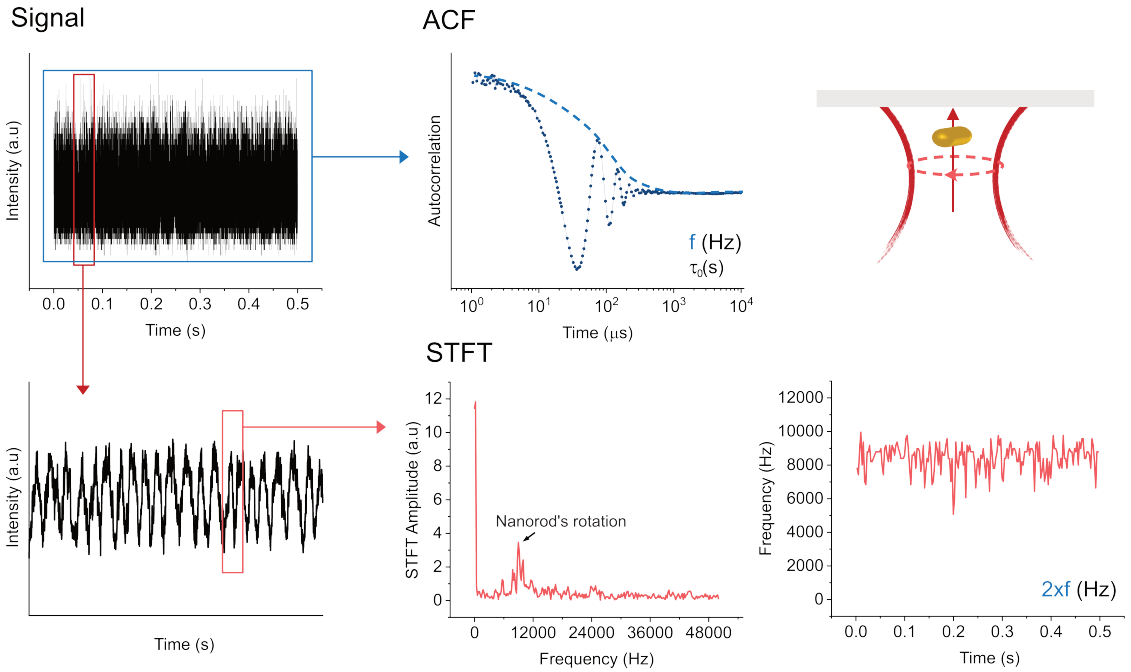

Figure 5.2: The signal contains information about the rotational dynamics of the optically trapped nanomotor. We analyze the signal using two methods: ACF and STFT. The ACF analysis correlates the signal from one measurement cycle, allowing us to determine the nanomotor's rotation frequency (f) and decay time (σ_0), which provides insights into the rotational Brownian motion of the nanomotor. The STFT analysis performs a discrete Fourier transform on segments of the signal, providing information about the nanomotor's rotation with higher temporal resolution. The nanomotor's rotation is indicated by a peak in the STFT amplitude at $2 \times f$. By extracting the frequency corresponding to this amplitude, we can determine the rotation frequency for the entire measurement cycle.

STFT is a frequency domain representation in which the signal is divided into shorter segments on which the Fourier transform is computed. This method is good when your signal has variations over time that would be average out if you used for example Discrete Fourier Transform (DFT) or Discrete-Time Fourier Transform (DTFT), which results in loss of information [99, 100].

The STFT is computed by sliding a window function $\omega[n]$ with length M over the signal $x[n]$ and calculating the DFT of each segment of the signal. The window function hops over the original signal at intervals of R, with a overlap of L=M-R between adjoining

segments. For a discrete signal the STFT is defined as

$$X[m,\omega] = \sum_{n=-\infty}^{\infty} x[n]\omega[n-m]e^{-j\omega n} \tag{5.3}$$

where m represent time index of the center of the window and n the time variable. The window functions vary, the most used one is the rectangular window function that just extracts the short sequence without modifications. Another window function is the Hanning window function. The Hanning window goes to zero, which generates a smoother transition between the sections and prevents spectral leakage. Spectral leakage occurs when a DFT of a signal causes energy from one frequency component to leak into other frequency bins. This is due to the DFT assuming that the signal is periodic, if that's not the case, spectral leakage may occur. Hence, one needs to consider which type of window is most suitable for the signal in question.

The backscattered light from the rotating rod generates data that is not very periodic, especially not when we trap the particle over a living cell. In our case is better to use the Hanning window, as it generates a better representation in frequency domain. Another parameter one need to consider is the length of the window, a shorter window generates a high resolution in time, but of the cost of blurring the frequency output, while a longer temporal window generates a sharp spectral resolution but of the expense of temporal resolution. For the data analyzed in this work we also need to consider the duration of the rod rotation. To be able to extract the displacement of the rod due to environmental changes (the cells motions) the rod must have taken at least one completed rotation, which means that the window needs to be at least as long as one rotation or longer. In our case the time window should be about 2 ms which corresponds to 10-20 complete revolutions.

5.1.2 Dark-Field Microscopy

Gold nanoparticles exhibit enhanced scattering and due to this, dark-field microscopy is often used for observation and imaging. In dark-field microscopy, the sample is illuminated with oblique or tangential light that pass though a dark-field oil immersion condenser. The scattered light is collected by the objective lens,

while transmitted light is excluded from the image, creating a dark background around the scattering sample structures.

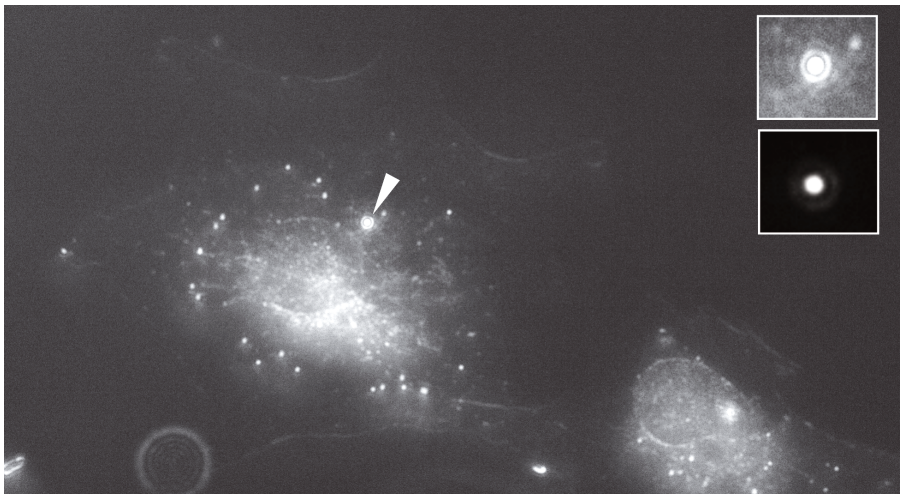

Figure 5.3: Dark-field microscopy image of endothelial cells, two smaller images of a trapped particle in cell media and in water are incorporated in the right corner. The scattering pattern from an endothelial cell reveals a homogeneous light scattering from the nucleus, which is clearly visible with its circular shape. Surrounding the nucleus, various organelles and vesicles scatter light slightly more intensely than the nucleus, providing a distinctive contrast. Moving further away from the nucleus, the visibility of scattering organelles diminishes, resulting in a region with significantly less scattering. At the absolute periphery of the cell, a very faint edge can be distinguished, outlining the cell's boundary. Marked with an arrow is an optically trapped gold nanoparticle, which stands out by scattering light significantly more than any part of the cell, making it easily identifiable against the background of cellular structures

Dark-field imaging of biological samples, such as cells, is also possible due to their variation in material density for different cellular compartments. Additionally, dark-field imaging is a non-invasive method that requires no dye, making it ideal for observing live cells without altering their natural state. When working with cells and gold nanoparticles, dark-field imaging is particularly advantageous because gold nanoparticles scatter light much more intensely than biological samples, making them easily distinguishable [80].

Figure 5.3 shows a dark-field image of two cells. In this image, we can observe the cells and their compartments. The cell membrane appears as a faint boundary, while the nucleus appears as a dense structure containing genetic material. Surrounding the nucleus is the cytoplasm, consisting of organelles and proteins, which may exhibit granules and vesicles. Distinguishing the nucleus and vesicles is easier compared to the membrane, especially in areas close to the

cell edge. This is because of the densely packed and curved nature of these structures membranes [101]. In Figure 5.3, structures resembling white dots appear in the cytoplasm around the nucleus; these are vesicles or granules. Due to their spherical shape and densely packed membrane, they scatter light much more effectively than an area in the peripheral cytoplasm where the cell membrane is more planar.

5.2 Gold Nanorod Synthesis and Functionalization

The LSPR of gold nanorods is highly dependent on their size and shape. Therefore, it is crucial to have a synthesis protocol that produces particles with high uniformity to ensure reproducibility for the methods developed in this thesis. The gold nanorods used in this work were synthesized by Dr. Lei Shao. Nanorods were prepared using a seeded growth method combined with anisotropic oxidation. This approach enhances control over the dimensions and uniformity of the nanorods, achieving better tunability and monodispersity. The detailed synthesis method can be found in the following references [102, 33].

The nanorods synthesized using this method have a bilayer of CTAB molecules, rendering them positively charged. However, CTAB has been shown to be toxic to cells at very low dosages [103, 104]. To prevent unwanted cell poisoning and reduce nanoparticle aggregation in cell media, the nanorods were functionalized with hydroxylated alkanethiols.

Chapter 6

Summary and Outlook

6.1 Summary and Integration of Findings

This thesis have explored optically trapped gold nanomotors and their applications in detecting mechanical cellular nanomotions. The previous chapters introduced the essential topics for the work presented in the appended paper. In Chapters 2 and 3, the fundamentals of plasmonics and optical tweezers are covered. The plasmonics chapter focused on how light interacts with metals, particularly nano-sized gold nanoparticles and localized surface plasmons (LSPs). In the optical tweezers chapter, the dipole approximation was used to derive the optical forces in an optical trap. In the same chapter, interaction between the trapping laser and the gold nanorod leads to its rotation was investigated. This occurs because the laser light transfers an enhanced optical torque to the nanorod through plasmonic effects, causing it to spin and function as what is referred to as a rotary nanomotor. In Chapter 4, endothelial cells was briefly introduced, which plays a key role in the appended paper and is the focus of the nanomotion detection study. In Chapter 5, the experimental approaches necessary to study the system discussed was presented.

Building on the fundamentals presented, the resulting paper can now be explored. In the appended paper, *Detecting nanomotion patterns of single endothelial cells using light-driven rotary nanomotors*, the relationship between the rotation of the nanomotor and its position along the optical axis of the laser beam was investigated. We found an almost linear relationship between the rotation frequency

and the position within the laser beam, resulting in a so-called *calibration curve*, which we utilized to convert changes in rotation frequency to changes in height, or displacements of the nanomotor. We then adapted our nanomotors for a biological environment by functionalizing them with thiols that prevented bonding to cell membranes. Thereafter, cells were introduced and the nanomotors were positioned at specific locations on top of the living cells, where they remained as the cells carried out their activities. As living organisms, cells are in constant motion, whether due to changes in shape or molecular motors transporting organelles or vesicles, all of which result in mechanical fluctuations within the cell. Using our method, we were able to measure these fluctuations. We found that we can measure mechanical nanomotions as small as 10 nm, over a highly localized area of 100×100 nm, with a temporal resolution of 2.5 ms. By analyzing the data using both ACF and STFT, we obtained information about the rods' rotation, particle temperature, and the properties of the surrounding medium. This approach demonstrates a promising method for probing the dynamic mechanical behavior of living cells at the nanoscale.

6.2 Future Work and Prospects

As we move forward, there are exciting prospects for enhancing and expanding the use of light-driven rotary nanomotors in various biological contexts, particularly in nanomotion detection. In the appended paper, we demonstrated the capability to measure highly localized nanomotions with sub-wavelength resolution. However, the specific cellular processes responsible for these nanomotions remain unknown, which could be addressed by incorporating a control method. In this case, fluorescence imaging would be used, where specific cellular compartments are dyed and tracked through video imaging, while measurements are simultaneously conducted with nanomotors. This approach would enable pinpointing the exact causes of different mechanical nanomotions. This opens up possibilities for more targeted analysis of biological processes. For example, one could study how nanomotions are related to cell viability, how the mechanical activity of specific cellular compartments is connected to their environment, or how these activities vary between different cell lines.

This highly sensitive method has already shown great potential as a biosensor in Dr. Jungová's work [30], where she studied the kinetic dynamics of DNA melting due to photothermal heating. The rigorously studied fundamentals of the nanomotor trapped in 2D, as presented in these works [28, 34, 35, 61, 63, 105], provide a solid foundation for further exploration of nanoscale systems, particularly in biological environments, which I find especially intriguing. Building on Dr. Jungová's work, one could investigate corona formation on the nanomotor when submerged in different biological fluids, potentially expanding our knowledge of diagnostic and therapeutic nanomedicine products.

Bibliography

1. Gest H. The discovery of microorganisms by Robert Hooke and Antoni van Leeuwenhoek, Fellows of The Royal Society. Notes and Records of the Royal Society of London 2004 May; 58:187–201
2. Seehausen O et al. Genomics and the origin of species. Nature Reviews Genetics 2014 Mar; 15:176–92
3. Williams CG et al. An introduction to spatial transcriptomics for biomedical research. Genome Medicine 2022 Jun; 14:68
4. Nielsen J and Keasling J. Engineering Cellular Metabolism. Cell 2016 Mar; 164:1185–97
5. Nair A et al. Conceptual Evolution of Cell Signaling. International Journal of Molecular Sciences 2019 Jul; 20:3292
6. D'Arcy MS. Cell death: a review of the major forms of apoptosis, necrosis and autophagy. Cell Biology International 2019 Jun; 43:582–92
7. Lichtman JW and Conchello JA. Fluorescence microscopy. Nature Methods 2005 Dec; 2:910–9
8. Sahl SJ et al. Fluorescence nanoscopy in cell biology. Nature Reviews Molecular Cell Biology 2017 Nov; 18:685–701
9. Wang T et al. Cellular Uptake of Nanoparticles by Membrane Penetration: A Study Combining Confocal Microscopy with FTIR Spectroelectrochemistry. ACS Nano 2012 Feb; 6:1251–9
10. McKinnon KM. Flow Cytometry: An Overview. Current Protocols in Immunology 2018 Jan; 120
11. Català-Castro F et al. Exploring cell and tissue mechanics with optical tweezers. Journal of Cell Science 2022 Aug; 135
12. Bustamante CJ et al. Optical tweezers in single-molecule biophysics. Nature Reviews Methods Primers 2021 Mar; 1:25
13. Roca-Cusachs P et al. Quantifying forces in cell biology. Nature Cell Biology 2017 Jul; 19:742–51
14. Wu PH et al. A comparison of methods to assess cell mechanical properties. Nature Methods 2018 Jul; 15:491–8
15. Ashkin A et al. Observation of a single-beam gradient force optical trap for dielectric particles. Optics Letters 1986 May; 11:288
16. Ashkin A. Acceleration and Trapping of Particles by Radiation Pressure. Physical Review Letters 1970 Jan; 24:156–9

17. Ashkin A et al. Optical trapping and manipulation of single cells using infrared laser beams. Nature 1987 Dec; 330:769–71

18. Bustamante C et al. Single-molecule studies of DNA mechanics. Current Opinion in Structural Biology 2000; 10:279–85

19. Svoboda K and Block SM. Force and velocity measured for single kinesin molecules. Cell 1994; 77:773–84

20. Brenner S et al. Force production of human cytoplasmic dynein is limited by its processivity. Science Advances 2020 Apr; 6

21. Wirtz D. Particle-Tracking Microrheology of Living Cells: Principles and Applications. Annual Review of Biophysics 2009 Jun; 38:301–26

22. Arbore C et al. Probing force in living cells with optical tweezers: from single-molecule mechanics to cell mechanotransduction. Biophysical reviews 2019; 11:765–82

23. Shinde A et al. A Review of Single-Cell Adhesion Force Kinetics and Applications. Cells 2021 Mar; 10:577

24. Svoboda K and Block SM. Optical trapping of metallic Rayleigh particles. Optics Letters 1994 Jul; 19:930

25. Toussaint KC et al. Plasmon resonance-based optical trapping of single and multiple Au nanoparticles. Optics Express 2007 Sep; 15:12017

26. Brzobohatý O et al. Three-Dimensional Optical Trapping of a Plasmonic Nanoparticle using Low Numerical Aperture Optical Tweezers. Scientific Reports 2015 Jan; 5:8106

27. Šiler M et al. Direct measurement of the temperature profile close to an optically trapped absorbing particle. Optics Letters 2016 Mar; 41:870

28. Odebo Länk N et al. Optical Tweezing and Photothermal Properties of Resonant Dielectric and Metallic Nanospheres. ACS Photonics 2020 Sep; 7:2405–12

29. Osinkina L et al. Tuning DNA Binding Kinetics in an Optical Trap by Plasmonic Nanoparticle Heating. Nano Letters 2013 Jul; 13:3140–4

30. Šípová H et al. Photothermal DNA Release from Laser-Tweezed Individual Gold Nanomotors Driven by Photon Angular Momentum. ACS Photonics 2018; 5:2168–75

31. Lehmuskero A et al. Ultrafast Spinning of Gold Nanoparticles in Water Using Circularly Polarized Light. Nano Letters 2013 Jul; 13:3129–34

32. Tong L et al. Alignment, Rotation, and Spinning of Single Plasmonic Nanoparticles and Nanowires Using Polarization Dependent Optical Forces. Nano Letters 2010 Jan; 10:268–73

33. Shao L et al. Gold nanorod rotary motors driven by resonant light scattering. ACS nano 2015; 9:12542–51

34. Lehmuskero A et al. Laser trapping of colloidal metal nanoparticles. ACS Nano 2015 Apr; 9:3453–69

35. Andrén D et al. Surface Interactions of Gold Nanoparticles Optically Trapped against an Interface. The Journal of Physical Chemistry C 2019 Jul; 123:16406–14

36. Novotny L and Hecht B. Principles of Nano-Optics. Cambridge University Press, 2012 Sep

37. Mark Fox. Optical Properties of Solids. 2nd ed. Oxford: Oxford University Press, Incorporated, 2010

38. Yang HU et al. Optical dielectric function of silver. Physical Review B - Condensed Matter and Materials Physics 2015 Jun; 91

39. Giannini V et al. Plasmonic nanoantennas: Fundamentals and their use in controlling the radiative properties of nanoemitters. 2011 Jun

40. Oubre C and Nordlander P. Optical Properties of Metallodielectric Nanostructures Calculated Using the Finite Difference Time Domain Method. The Journal of Physical Chemistry B 2004 Nov; 108:17740–7

41. Johnson PB and Christy RW. Optical Constants of the Noble Metals. Physical Review B 1972 Dec; 6:4370–9

42. Maier SA. Plasmonics: Fundamentals and Applications. Springer Science + Business Media LLC, 2007

43. Sepúlveda B et al. LSPR-based nanobiosensors. Nano Today 2009 Jun; 4:244–51

44. Xu T and Geng Z. Strategies to improve performances of LSPR biosensing: Structure, materials, and interface modification. Biosensors and Bioelectronics 2021 Feb; 174:112850

45. Myroshnychenko V et al. Modelling the optical response of gold nanoparticles. Chemical Society Reviews 2008 Aug; 37:1792–805

46. Meier M and Wokaun A. Enhanced fields on large metal particles: dynamic depolarization. Optics Letters 1983 Nov; 8:581

47. Ellen Zeman CJ and Schatz GC. An Accurate Electromagnetic Theory Study of Surface Enhancement Factors for. Tech. rep. 1987 :634–43

48. Bohren CF and Huffman DR. Absorption and Scattering of Light by Small Particles. John Wiley & Sons, Inc., 1983

49. Dara P et al. Directional Control of Transient Flows Generated by Thermoplasmonic Bubble Nucleation. The Journal of Physical Chemistry C 2023 Sep; 127:17454–9

50. Jones S et al. Ultrafast Modulation of Thermoplasmonic Nanobubbles in Water. Nano Letters 2019 Nov; 19:8294–302

51. Braun M et al. Single Molecules Trapped by Dynamic Inhomogeneous Temperature Fields. Nano Letters 2015 Aug; 15:5499–505

52. Huang X et al. Plasmonic photothermal therapy (PPTT) using gold nanoparticles. Lasers in Medical Science 2008 Jul; 23:217–28

53. Tian Q et al. Hydrophilic Cu9S5 Nanocrystals: A Photothermal Agent with a 25.7% Heat Conversion Efficiency for Photothermal Ablation of Cancer Cells in Vivo. ACS Nano 2011 Dec; 5:9761–71

54. Baffou G and Quidant R. Thermo-plasmonics: using metallic nanostructures as nano-sources of heat. Laser & Photonics Reviews 2013 Mar; 7:171–87

55. Jones PH et al. Optical Tweezers: Principles and Applications. Cambridge University Press, 2015

56. Arias-González JR and Nieto-Vesperinas M. Optical forces on small particles: attractive and repulsive nature and plasmon-resonance conditions. Journal of the Optical Society of America A 2003 Jul; 20:1201

57. Neuman KC and Block SM. Optical trapping. Review of Scientific Instruments 2004 Sep; 75:2787–809

58. Einstein A. Über die von der molekularkinetischen Theorie der Wärme geforderte Bewegung von in ruhenden Flüssigkeiten suspendierten Teilchen. Annalen der Physik 1905 Jan; 322:549–60

59. Fogel'son RL and Likhachev ER. Temperature dependence of viscosity. Technical Physics 2001 Aug; 46:1056–9

60. Purcell EM. Life at low Reynolds number. American Journal of Physics 1977 Jan; 45:3–11

61. Hajizadeh F et al. Brownian fluctuations of an optically rotated nanorod. Optica 2017; 4:746–51

62. Israelachvili JN. Intermolecular and Surface Forces. 3rd ed. Elsevier, 2011

63. Šípová-Jungová H et al. Nanoscale Inorganic Motors Driven by Light: Principles, Realizations, and Opportunities. Chemical Reviews 2020 Jan; 120:269–87

64. Lee YE et al. Optical torque from enhanced scattering by multipolar plasmonic resonance. Nanophotonics 2014 Dec; 3:343–50

65. Kong D et al. Swimming motion of rod-shaped magnetotactic bacteria: the effects of shape and growing magnetic moment. Frontiers in Microbiology 2014; 5

66. Alberts B et al. Molecular biology of the cell. 6th ed. New York: Garland Science, 2015

67. Bouïs D et al. Endothelium in vitro: A review of human vascular endothelial cell lines for blood vessel-related research. Angiogenesis 2001; 4:91–102

68. Favero G et al. Endothelium and Its Alterations in Cardiovascular Diseases: Life Style Intervention. BioMed Research International 2014; 2014:1–28

69. Libby P et al. Progress and challenges in translating the biology of atherosclerosis. Nature 2011 May; 473:317–25

70. Vanhoutte PM et al. Endothelial dysfunction and vascular disease. Acta Physiologica 2009 Jun; 196:193–222

71. Kolka CM and Bergman RN. The endothelium in diabetes: Its role in insulin access and diabetic complications. Reviews in Endocrine and Metabolic Disorders 2013 Mar; 14:13–9

72. McGranahan N and Swanton C. Biological and Therapeutic Impact of Intratumor Heterogeneity in Cancer Evolution. Cancer Cell 2015 Jan; 27:15–26

73. Kruse K and Jülicher F. Oscillations in cell biology. Current Opinion in Cell Biology 2005 Feb; 17:20–6

74. Martin P et al. Spontaneous Oscillation by Hair Bundles of the Bullfrog's Sacculus. The Journal of Neuroscience 2003 Jun; 23:4533–48

75. Küppers M et al. Confocal interferometric scattering microscopy reveals 3D nanoscopic structure and dynamics in live cells. Nature Communications 2023 Apr; 14:1962

76. Nixon-Abell J et al. Increased spatiotemporal resolution reveals highly dynamic dense tubular matrices in the peripheral ER. Science 2016 Oct; 354

77. Biswas A et al. Mapping Cell Membrane Fluctuations Reveals Their Active Regulation and Transient Heterogeneities. Biophysical Journal 2017 Oct; 113:1768–81

78. Nolte DD. Coherent light scattering from cellular dynamics in living tissues. Reports on Progress in Physics 2024 Mar; 87:036601

79. Soh S et al. Reaction-Diffusion Systems in Intracellular Molecular Transport and Control. Angewandte Chemie International Edition 2010 Jun; 49:4170–98

80. Nan X et al. Organelle Tracking in a Living Cell with Microsecond Time Resolution and Nanometer Spatial Precision. ChemPhysChem 2008 Apr; 9:707–12

81. Kural C et al. Kinesin and Dynein Move a Peroxisome in Vivo: A Tug-of-War or Coordinated Movement? Science 2005 Jun; 308:1469–72

82. Nicholas MP et al. Control of cytoplasmic dynein force production and processivity by its C-terminal domain. Nature Communications 2015 Feb; 6:6206

83. Schnitzer MJ and Block SM. Kinesin hydrolyses one ATP per 8-nm step. Nature 1997 Jul; 388:386–90

84. Niescier RF et al. Dynamics of Mitochondrial Transport in Axons. Frontiers in Cellular Neuroscience 2016 May; 10

85. Umeshima H et al. Microtubule-based nuclear movement occurs independently of centrosome positioning in migrating neurons. Proceedings of the National Academy of Sciences 2007 Oct; 104:16182–7

86. Martini FJ and Valdeolmillos M. Actomyosin Contraction at the Cell Rear Drives Nuclear Translocation in Migrating Cortical Interneurons. Journal of Neuroscience 2010 Jun; 30:8660–70

87. Burridge K et al. Focal Adhesions: Transmembrane Junctions Between the Extracellular Matrix and the Cytoskeleton. Annual Review of Cell Biology 1988 Nov; 4:487–525

88. Turlier H et al. Equilibrium physics breakdown reveals the active nature of red blood cell flickering. Nature Physics 2016 May; 12:513–9

89. Lane J and Allan V. Microtubule-based membrane movement. Biochimica et Biophysica Acta (BBA) - Reviews on Biomembranes 1998 Jun; 1376:27–55

90. Merrifield CJ et al. Imaging actin and dynamin recruitment during invagination of single clathrin-coated pits. Nature Cell Biology 2002 Sep; 4:691–8

91. Stupar P et al. Nano-Motion Analysis for Rapid and Label Free Assessing of Cancer Cell Sensitivity to Chemotherapeutics. Medicina 2021 May; 57:446

92. Li Z et al. Intracellular optical doppler phenotypes of chemosensitivity in human epithelial ovarian cancer. Scientific Reports 2020 Oct; 10:17354

93. Lissandrello C et al. Nanomechanical motion of Escherichia coli adhered to a surface. Applied Physics Letters 2014 Sep; 105

94. Rosłoń IE et al. Probing nanomotion of single bacteria with graphene drums. Nature nanotechnology 2022; 17:637–42

95. Kohler AC et al. Nanomotion detection based on atomic force microscopy cantilevers. The Cell Surface 2019; 5:100021

96. Willaert RG et al. Single yeast cell nanomotions correlate with cellular activity. Science advances 2020; 6:eaba3139

97. Nolte DD et al. Tissue dynamics spectroscopy for phenotypic profiling of drug effects in three-dimensional culture. Biomedical Optics Express 2012 Nov; 3:2825

98. Oppenheim AV et al. Signals and systems. 2nd ed. Harlow, Essex: Pearson Education Ltd, 2014

99. Cohen L. Time-frequency analysis. Vol. 778. Prentice Hall PTR New Jersey, 1995

100. Gupta V and Mittal M. Respiratory signal analysis using PCA, FFT and ARTFA. *2016 International Conference on Electrical Power and Energy Systems (ICEPES)*. IEEE, 2016 :221–5

101. Suissa M et al. Internal dynamics of a living cell nucleus investigated by dynamic light scattering. The European Physical Journal E 2008 Aug; 26:435

102. Ye X et al. Using Binary Surfactant Mixtures To Simultaneously Improve the Dimensional Tunability and Monodispersity in the Seeded Growth of Gold Nanorods. Nano Letters 2013 Feb; 13:765–71

103. Alkilany AM and Murphy CJ. Toxicity and cellular uptake of gold nanoparticles: what we have learned so far? Journal of Nanoparticle Research 2010 Sep; 12:2313–33

104. Alkilany AM et al. Cellular Uptake and Cytotoxicity of Gold Nanorods: Molecular Origin of Cytotoxicity and Surface Effects. Small 2009 Mar; 5:701–8

105. Andren D et al. Probing photothermal effects on optically trapped gold nanorods by simultaneous plasmon spectroscopy and brownian dynamics analysis. ACS nano 2017; 11:10053–61